POISSON PROCESS STIMULATION OF AN EXCITABLE MEMBRANE CABLE MODEL

M. D. GOLDFINGER
Department of Physiology and Biophysics, School of Medicine and College of Science & Engineering, Wright State University, Dayton, Ohio, 45401-0927

ABSTRACT The convergence of multiple inputs within a single-neuronal substrate is a common design feature of both peripheral and central nervous systems. Typically, the result of such convergence impinges upon an intracellularly contiguous axon, where it is encoded into a train of action potentials. The simplest representation of the result of convergence of multiple inputs is a Poisson process; a general representation of axonal excitability is the Hodgkin-Huxley/cable theory formalism. The present work addressed multiple input convergence upon an axon by applying Poisson process stimulation to the Hodgkin-Huxley axonal cable. The results showed that both absolute and relative refractory periods yielded in the axonal output a random but non-Poisson process. While smaller amplitude stimuli elicited a type of short-interval conditioning, larger amplitude stimuli elicited impulse trains approaching Poisson criteria except for the effects of refractoriness. These results were obtained for stimulus trains consisting of pulses of constant amplitude and constant or variable durations. By contrast, with or without stimulus pulse shape variability, the post-impulse conditional probability for impulse initiation in the steady-state was a Poisson-like process. For stimulus variability consisting of randomly smaller amplitudes or randomly longer durations, mean impulse frequency was attenuated or potentiated, respectively. Limitations and implications of these computations are discussed.

INTRODUCTION

The convergence of electrical activity generated by multiple inputs upon, or by multiple active sites within, a single neuron is a common design feature in the nervous system. Such disparate elements as a central neuron—with its many individual input synaptic terminals—and a cutaneous primary afferent axon—with its many individual mechanoreceptor terminal branches—share the inherent feature of being a substrate for the merging of respective types of electrical activity. The diversity of substrate structure (i.e., electronic configuration) and converging waveforms (post-synaptic, generator, and impulse currents) implies a diversity of possible types of convergence. However, two general principles are evident.

First, the simplest type of multiple-source convergence would involve inputs of equal amplitude and very short duration (such that individual events were nonsuperimposable). Then, whatever the sequence of input occurrences, the merged result is the well-known Poisson process (Cox and Smith, 1953; Cox and Miller, 1965). The fundamental property of this stochastic point process is that the probability P of an event in the sequence of events generated by the merging of inputs is a constant: $P(t) = R\,dt$, where R is the stationary mean rate (Griffith, 1971).

The second general principle is that the output process due to convergence impinges upon a length of excitable membrane cable ('nonspiking neurons' [Roberts and Bush, 1981] being an exception). Two examples are the neuronal axon hillock and the first node of a mechanoreceptor afferent unit's parent axon. While such sites may be spatially separate from the actual substrate of activity convergence (e.g., Moore et al., 1983), their common function is the initiation of a sequence of impulses stimulated by the input convergence process.

Thus, the simplest model of the transformation of multi-source activity convergence into a singular impulse-encoded process is represented by the stimulation of a length of excitable membrane cable by a Poisson sequence of stimuli; this is the subject of the present work. The Hodgkin-Huxley axon (Hodgkin and Huxley, 1952) was used as a general model for excitable membrane cable responses. A Poisson process (nuclear disintegration) was used to represent the general result of convergence as trains of stimulus pulses whose amplitudes and durations were either fixed or varied randomly in respective runs. The resultant elicited trains of impulses were analyzed as a point process, whose stochastic properties were compared with those of the input process. The objective of this work was to provide a general description of the transformation from Poisson stimulus sequence to output impulse train.

METHODS

The numerical computation methods used for the Hodgkin-Huxley axon were conventional and described elsewhere (Goldfinger, 1978). The benchmark test of suitability of the numerical method for spatial and temporal integration (modified Euler) was based upon the ability to reconstruct the conduction velocity vs. fiber diameter data of Pumphrey

and Young (1938) for cephalopod axons. The following cable parameters were used throughout: cable diameter = 100 μm; temperature = 10°C; internal resistivity = 34.5 Ωcm (Rall, 1977); membrane capacity = 1.0 μF/cm^2. Maximal ionic conductances were 120., 36., and 0.3 mmho/cm^2 for Na, K, and leakage channels, respectively. Equilibrium potentials were +55., −72, and −49.4 mV for Na, K, and leakage currents, respectively. Resting potential was −60 mV. Initial values of conductance parameters m, n, and h were 0.053, 0.320, and 0.596, respectively (Hodgkin and Huxley, 1952). Spatial, electrotonic, and temporal integration steps were: 406 μm, 0.125 space constant, and 10 μs, respectively. Cables studied had total electrotonic length Z (i.e., axial length normalized to the 3,245 μm space constant: Rall, 1977) of 0.5, 1.0, 2.0, or 3.0. Impulse conduction velocity was 4.9 M/s. Computations were performed on a PDP VAX 11/780 (Z = 0.5; 1.0 runs) or a PDP 11/34A (Z = 2.0; 3.0 runs).

To adequately represent the output (impulse train) parent process, each Poisson stimulation run was sustained continuously until at least 950 impulses were generated. To shorten the computation time, the voltage-dependent rate constants were preevaluated at 1 mV increments over the operating range of −80 mV to +60 mV., and stored in a look-up table (Hines, 1984). The shape and conduction velocity of an action potential thus computed were nearly identical to those found by evaluating the rate constants in each iteration. In all runs, stimulus and impulse occurrence times were translated into sequential interevent intervals and stored on disk for subsequent analysis.

For Poisson stimulation, the waiting time for the next successive stimulus occurrence was determined by an equiprobable random selection from a stack of 2,011 event intervals originally generated by a Poisson process (nuclear disintegration: Goldfinger, 1984*a*,*b*). This discrete-time stimulus process had a mean rate of 97.56/s (= average value over the 44

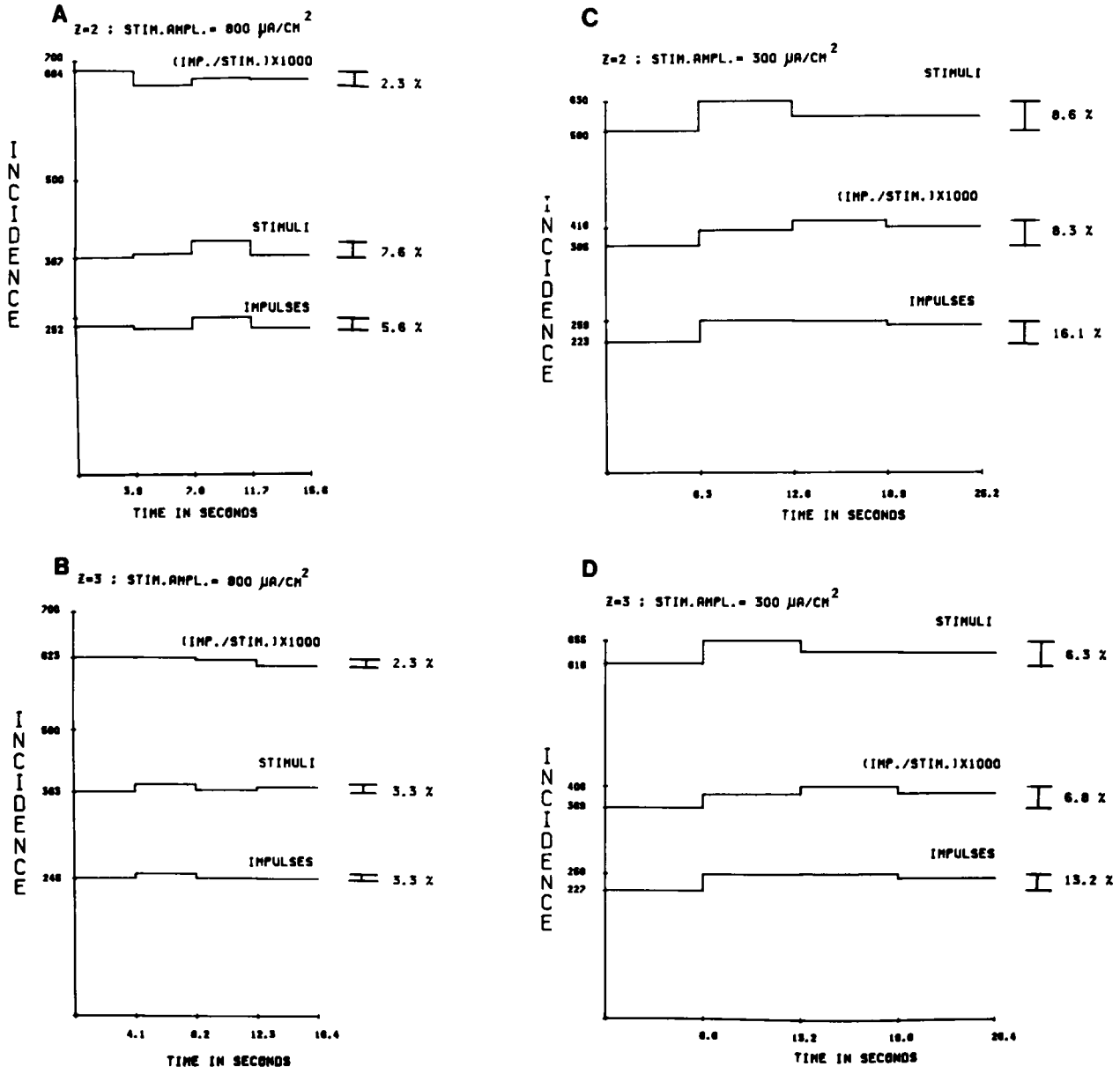

FIGURE 1 Stability testing. Each of the four representative runs was divided into four consecutive times segments of equal duration. Plotted for each segment are the number of stimuli, the number of impulses, and the ratio of impulses to stimuli (IMP/STIM) multiplied by 1,000. To the right of each plot is given the greatest departure of any segment's value relative to the value of the first segment.

runs of this study); the standard deviation between the mean rates of all runs was 1.79/s. The average coefficient of variation was 0.972, and varied with standard deviation of 0.020, over all runs. The stochastic properties of this stimulus process are described below (Results; Fig. 4). In the simplest stimulus trains, each successive stimulus consisted of a 0.2 ms-duration rectangular outward current pulse, whose amplitude was constant for a given run. In other runs, stimulus pulse amplitude and/or duration were varied (Fig. 6). Each successive stimulus was applied to one end of the cable. Each initiated action potential was detected either at the end of the cable (Z = 0.5, 1.0 runs) or at a point 1.5 space constants from the stimulated end (Z = 2.0, 3.0 runs). Impulse occurrence was detected by amplitude and shape discrimination of the membrane potential trajectory at the recording site; occasional 'stimulus artifacts' were thus excluded from detection.

For both input stimulus and output impulse data (sequential event times), two stochastic estimators were used to characterize features of respective point processes. First, the Interevent Interval Distribution —'*IID*'—was constructed; its mean interval and standard deviation were computed. The *IID* coefficient of variation was corrected for the deadtime (Goldfinger and Amassian, 1980). The reciprocal of the *IID* mean interval was used as the mean event frequency. Second, as a real-time estimator of event train patterns, the Expectation Density '*ED*' (Poggio and Viernstein, 1964) was computed. The *ED* is analogous to an autocorrelation function and represents a post-event occurrence histogram. While the *ED* of a statistically-stable periodic process has periodicity, the *ED* of a Poisson process has a constant mean level proportional to the mean frequency (ibid.). The mean and standard deviation of each *ED*'s noisy envelope were subsequently computed for the steady-state (T = 50–100 ms) only.

Statistical stability of both input stimulus and output impulse trains was assessed by comparing train parameters for consecutive isochronal segments of the run (Goldfinger and Amassian, 1980). Each segment had a duration equal to one fourth of the duration of the entire run. Four examples are shown in Fig. 1; maximal percent changes over the run were assessed with respect to the first time segment. The Poisson stimulus sequence did not vary above 9% of its initial rate. Greater variations in mean rate for the corresponding impulse sequences were due to (*a*) the relatively small number of impulses in a given segment being an inadequate sample of the parent probability density function, (*b*) the statistical variability of that segment's stimulus sequence. However, the ratio of number of impulses to number of stimuli during successive segments did not vary above 9%. In addition, neither the deadtime value (i.e., minimum interimpulse interval) nor the shape of the *ED* changed appreciably over consecutive segments. These observations indicated that the computations exhibited acceptable statistical stability, a necessary condition for the assumption of stationarity required for point process

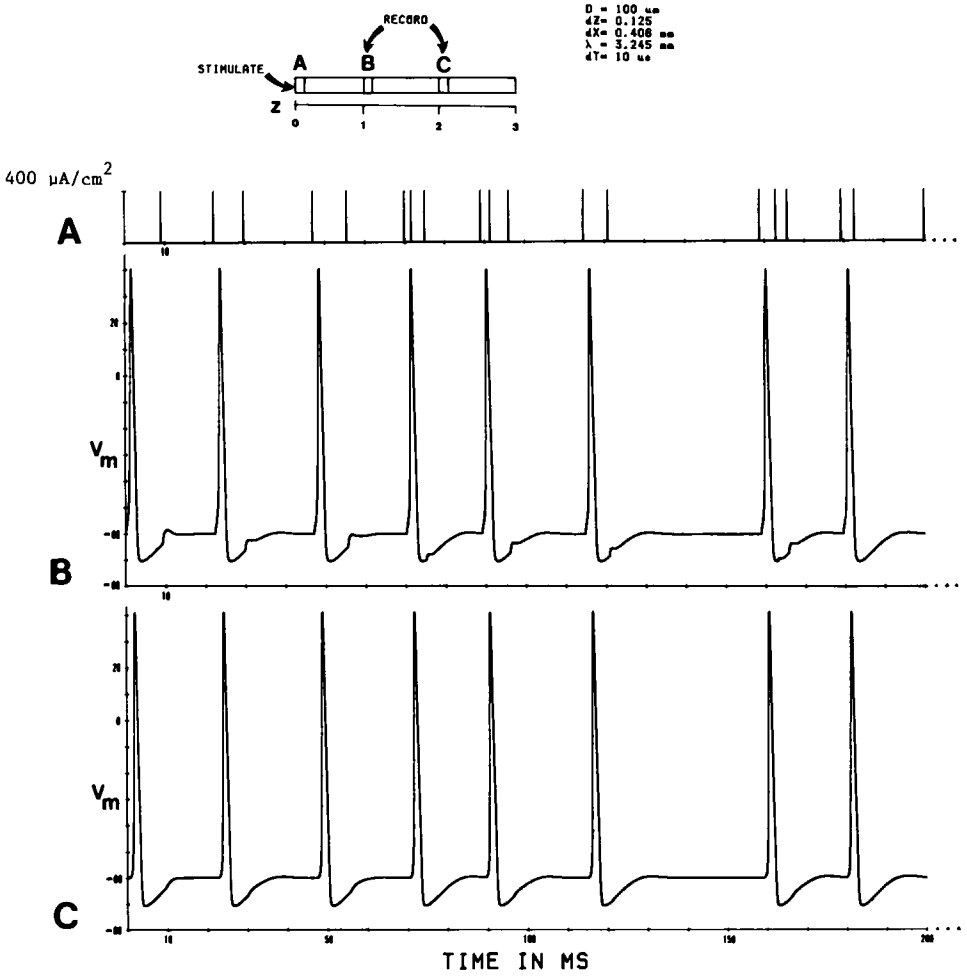

FIGURE 2 Example of computed output. Cable configuration is shown at top; Z is axial distance normalized to the space constant. Stimuli (each at 0.2 ms duration, 400 $\mu A/cm^2$ amplitude) were delivered to one end (*A*; stimulus train in record *A*). Trajectories of membrane potential (Vm) were recorded here at two distal points (B,C; records *B* and *C*, respectively). Record *B* shows effects of stimuli that did not initiate an impulse at point *A*. Computation, shown here for its first 200 ms, was sustained until 1,000 impulses were initiated. All stimulus and impulse occurrence times are translated into sequential inter-event intervals for subsequent point process analysis.

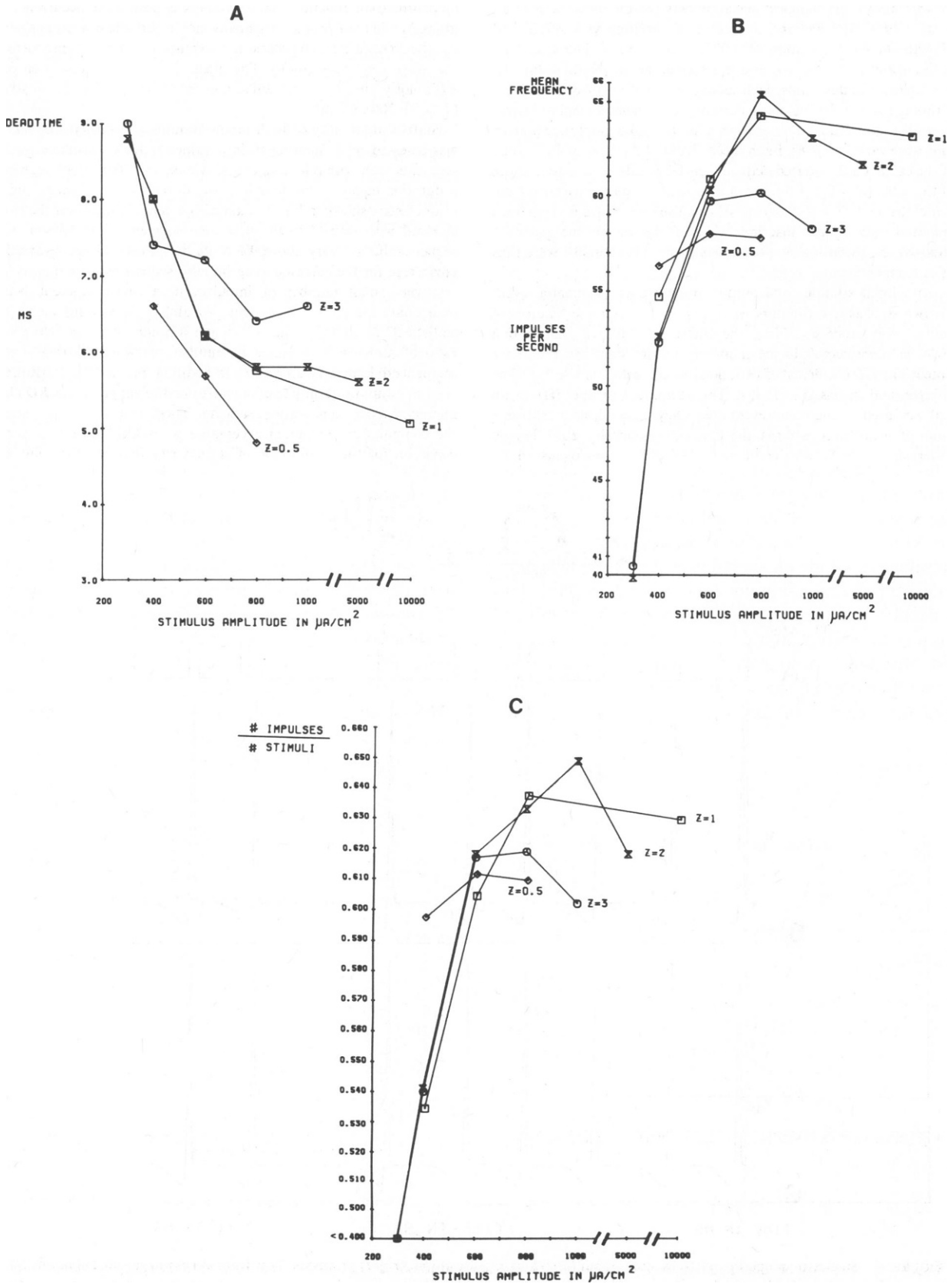

FIGURE 3 Effects of stimulus amplitude on (*A*) deadtime (– minimal interimpulse interval value), (*B*) mean impulse frequency (– reciprocal of mean interimpulse interval), and (*C*) number of impulses normalized to the number of stimuli delivered. Note nonzero origins and discontinuous abscissae. *Z* values indicate total electrotonic length of the cable.

analysis (Cox and Lewis, 1966). Such stability also suggested—but did not prove—that for these necessarily long computations, accumulated computational errors were negligible.

RESULTS

Poisson Trains of Invariant Stimulus Pulses

In these computations, a Poisson sequence of stimulus pulses was applied to the excitable cable model. Each stimulus pulse had a 0.2 ms duration and a fixed amplitude. A sample of the response of the model axon to this type of Poisson stimulation is shown in Fig. 2. All stimulus pulses were equivalent except for their respective time of occurrence (record A). Impulses initiated at the end of the cable propagated to the recording site(s). When observed close to the stimulated end (e.g., record B), membrane potential trajectories showed electrotonic potential changes associated with the failure of impulse initiation at the stimulation site. Impulse initiation typically failed for the second of a pair of short-interval stimuli. However, larger amplitude stimuli promoted impulse initiation at shorter interstimulus intervals.

Fig. 3 illustrates for separate runs the potentiating effect of stimulus amplitude on short-interval impulse initiation. The deadtime (i.e., minimum interimpulse interval, Fig. 3 *A*) declined with greater stimulus amplitude. While the effect was ultimately limited by the absolute refractory period, stimulus shunting by the cable electrotonic load additionally increased the minimum interimpulse interval elicited by a given stimulus amplitude. Similarly, larger stimulus amplitude increased the occurrence of other classes of relatively short interimpulse intervals and thereby increased the mean firing frequency (Fig. 3 *B*), an effect that was independent of the actual number of stimuli (Fig. 3 *C*). However, at the highest stimulus amplitudes, mean firing rate could be less than that elicited by a lower stimulus amplitude (despite the shorter deadtime). This paradoxical effect was due to the tendency for larger stimuli to generate the shortest intervals: their occurrence decreased the probability of a subsequent impulse initiation, via the refractoriness associated with the second of a short-interval impulse pair. (This effect is explained more clearly with the *ED* function, described below.)

The entire stochastic process during Poisson stimulation is illustrated in Fig. 4 for a representative run. The Poisson nature of the stimulus process (left) was shown by steady-state (*IID*) and real-time (*ED*) estimators. The *IID* had a single-exponential falling limb; the *IID* log-ordinate plot was well-fit ($r > 0.9$) by the regression line (computed between $T = 1$–32 ms) whose slope (= 9.8 ms) approximated the *IID* mean interval value (= 10.1 ms) less the deadtime (= 0.3 ms). The *ED* of the stimulus process was essentially a constant within the bounds of a noisy envelope defined here as ± one standard deviation of the steady-state ($T = 50$–100 ms) ordinate values. The value of the *ED* steady-state ordinate mean equaled 98.3% of the value predicted from the *IID* mean interval (Poggio and Viernstein, 1964).

The impulse output process (right) differed from the stimulus input process (left). In the *IID*, the longer dead-

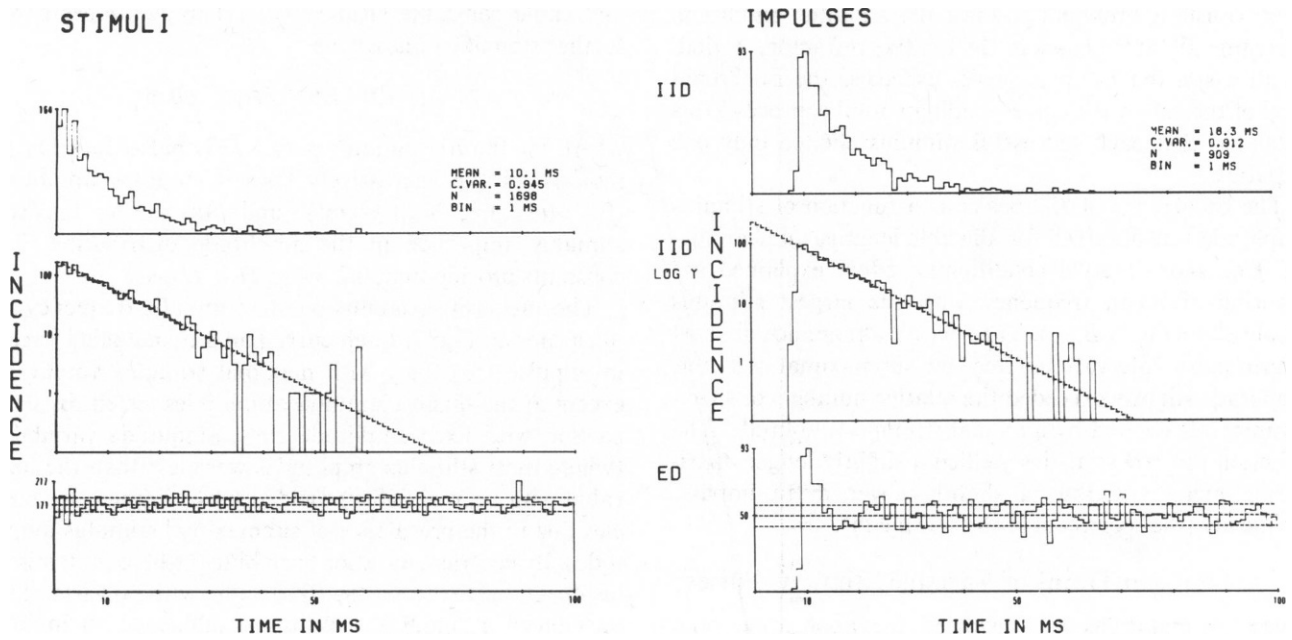

FIGURE 4 Stochastic properties of the stimulus input (*left*) and impulse output (*right*) processes. *Top:* Inter-event interval distribution (*IID*) linear ordinate plot. *Middle: IID*-Log Ordinate plot; linear regression on the falling limb (broken line) was computed over the largest content contiguous bins (*left*, bins 1–32; *right*, bins 10–35). *Bottom:* Expectation Density (*ED*); dotted horizontal lines represent ordinate levels of mean with +/− one standard deviation of the noisy envelope computed over the latter half of the function (bins 50–100). All plots have 1 ms binwidths. Respective mean frequencies were: 99.01/s for stimuli; 54.65/s for impulses.

time was followed by a fast rise to the distribution peak. Subsequent to the peak (mode), the *IID* fell off as a nearly single exponential; the regression (computed between T = 10–35 ms, the range of value which included most of the intervals) had a slope of 9.46 ms, which differed from the *IID* mean interval less the deadtime (= 8 ms) by 8%. Nevertheless, the impulse process for intervals greater than 10 msec was not a Poisson process: where the *IID* was linear on the log-ordinate plot, the *ED* was not a constant (i.e., not within the steady-state envelope). The *ED* showed an early (post-deadtime) peak which greatly exceeded the steady-state noisy envelope.

This *ED* peak was related to stimulus amplitude, as is shown in Fig. 5. With increasing stimulus amplitude, the *ED* was changed. As the deadtime decreased, the *ED* peak occurred earlier with respect to the function's origin. An essentially infinite stimulus amplitude (e.g., Fig. 5 *B*, Z = 1: 10,000 μA/cm^2; Fig. 5 *C*, Z = 3: 1,000 μA/cm^2) eliminated the *ED* peak. Thus, the *ED* peak revealed a (non-Poisson) aspect of impulse initiation, where larger stimulus amplitudes could 'overcome' earlier phases of the relative refractory period. With smaller stimuli, the shortest possible interimpulse intervals were not generated; this deficit enhanced the probability of impulse initiation at intervals slightly longer than the deadtime, hence the *ED* peak. Intervals just longer than the *ED* peak extent occurred with reduced probability due to the refractoriness imposed by the short interval conditioning indicated by the *ED* peak. This effect gave the *ED* trajectory the appearance of a damped oscillation (e.g., Fig. 5 *D*, Z = 3, 300 μA/cm^2 record). Thereafter, intervals occurred with essentially constant probability, since the stimulus amplitude overcame all later phases of the relative refractory period. In all cases, the *ED* peak never exceeded the isochronal level of the *ED* of the corresponding stimulus process; this indicated that each successful stimulus elicited only one impulse.

The occurrence of *ED* peaks as a function of stimulus amplitude was observed for all cable lengths studied (Fig. 5). This short-interval conditioning effect explained the lowering of mean frequency with the largest stimulus amplitudes (Fig. 3 *B*, *C*). The relative abundance of short interimpulse intervals elicited by submaximal stimulus amplitude slightly exceeded the relative numbers of shortest intervals elicited by maximal stimulus amplitude. The effect on the *IID* statistics yielded a slightly longer distribution mean and thus a slightly lower mean impulse frequency (the reciprocal of the *IID* mean).

Poisson Trains of Variable Stimulus Pulses

These computations also involved the application of a Poisson sequence of stimulus pulses to the excitable cable model, with the addition of variability of stimulus shape parameters. A cable electrotonic length of 2 was used, so that the effects of variability were assessed sufficiently distal (at Z = 1.5) to the stimulated end, with no complications introduced by electrotonic transients. In separate runs, either stimulus amplitude or duration or both were varied sequentially and randomly. Variability was generated for each successive stimulus by an equiprobable selection from the distributions shown in Fig. 6.

The sample duration distribution (Fig. 6 *A*) represented a parent distribution of constant incidence of durations between 0.2 ms (i.e., that used in runs without duration variability) and 2.0 ms. The upper limit of durations was arbitrarily chosen to provide a 10-fold span of durations, while minimizing the random mismatch between an interstimulus interval shorter than the duration of the first stimulus of the pair. (Such rare occurrences were treated by postponing the onset of the second stimulus until the end of the first stimulus.)

The sample amplitude distribution (Fig. 6 *B*) similarly represented a parent distribution of constant incidence of amplitudes between >0 and twice the mean amplitude. The process of successive parameter selection is illustrated for amplitude variability in Fig. 6 *C*. The upper trace shows the amplitudes of 100 successive stimulus pulses, where much variability was evident. However, averaging 10 such episodes in succession (lower trace) showed that the averages centered about the distribution mean.

One series of runs sought to introduce both amplitude and duration variability. For each successive stimulus, an amplitude was selected as described. An inverse relationship between stimulus amplitude and duration was assumed, by analogy with the amplitude-duration relation for postsynaptic potentials initiated at different points of an equivalent core conductor of homogeneous geometry and cable constants (Rall, 1977). This relationship was further simplified linearly as

$$Ti = [-1.8 \cdot (Ai/Am)] + 2.0 \text{ ms},$$

where for the ith stimulus pulse: Ti is pulse duration (in ms), Ai is the successively chosen stimulus amplitude ($0 < Ai \leq Am$, in μA/cm^2), and Am is the maximal stimulus amplitude in the amplitude distribution. The constants provide that: 0.2 ms $\leq Ti <$ 2. ms.

The effects of variability on mean impulse frequency are illustrated in Fig. 7. Each curve had a monotonic increase in impulse frequency with maximal stimulus amplitude, except at the highest stimulus amplitudes tested. By comparison with fixed-amplitude runs, amplitude variability (where most stimulus amplitudes were less than the fixed value with no variability) yielded lower impulse frequencies due to the prevalence of submaximal stimulus amplitudes. By contrast, duration variability (where most stimulus durations exceeded the fixed value with no variability) introduced a significant excitatory influence on impulse frequencies elicited without variability at lower (<600 μA/cm^2) maximal stimulus amplitudes. With dual-parameter (i.e., amplitude-and-duration) variability, the impulse frequency curve was between that from either variability alone. At higher maximal stimulus amplitudes (>500

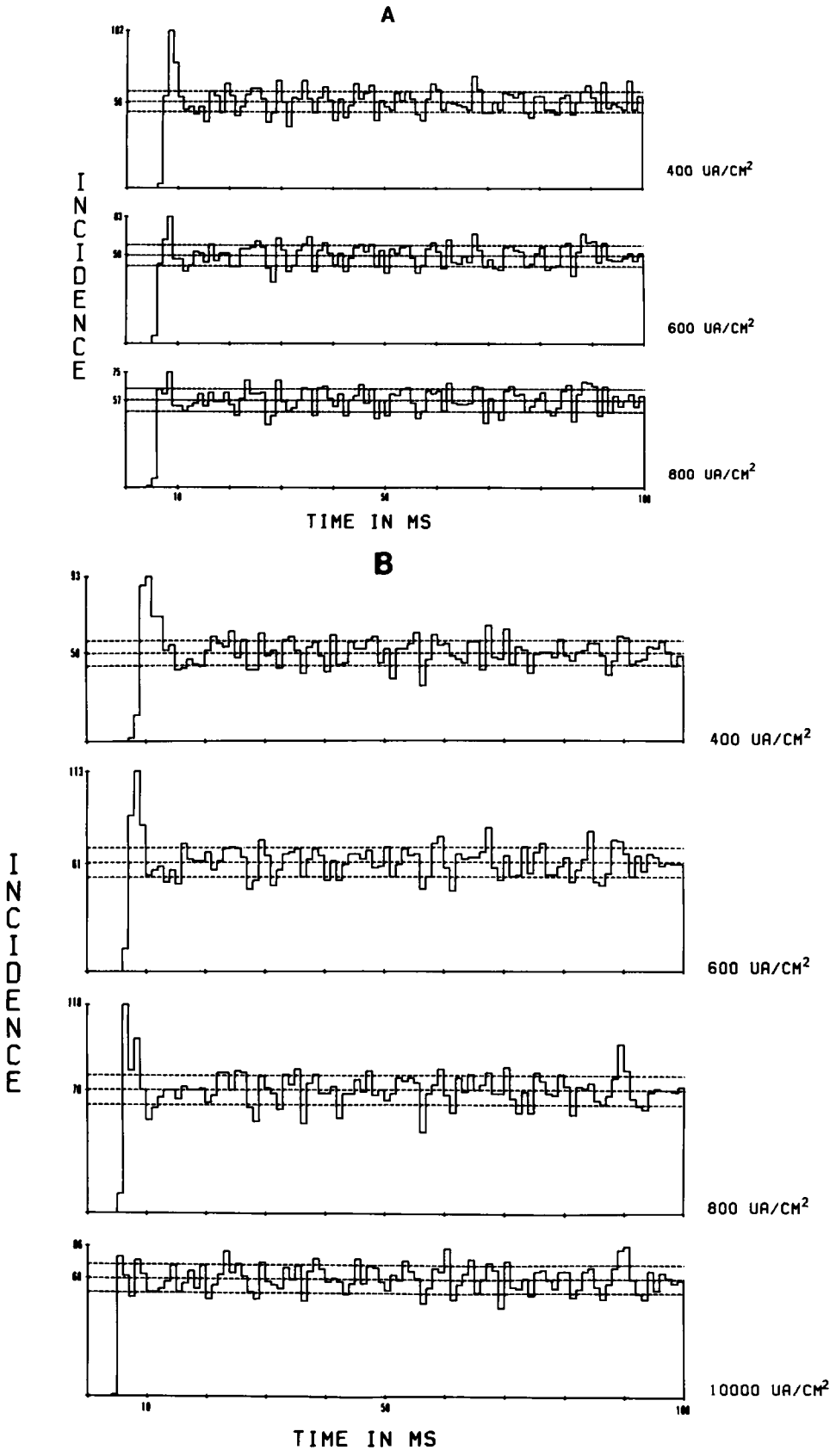

FIGURE 5 Changes in *ED* trajectories with stimulus amplitude. Values of *Z* (total electronic length) were: (*A*), 0.5; (*B*), 1.0; (*C*), 2.0; (*D*), 3.0. Dashed lines show ordinate mean and +/− one standard deviation of the envelope of the latter half of the function (bins 50–100). All plots have 1 ms binwidth. All runs contained at least 950 impulses. Statistical stability was assessed as per Fig. 1.

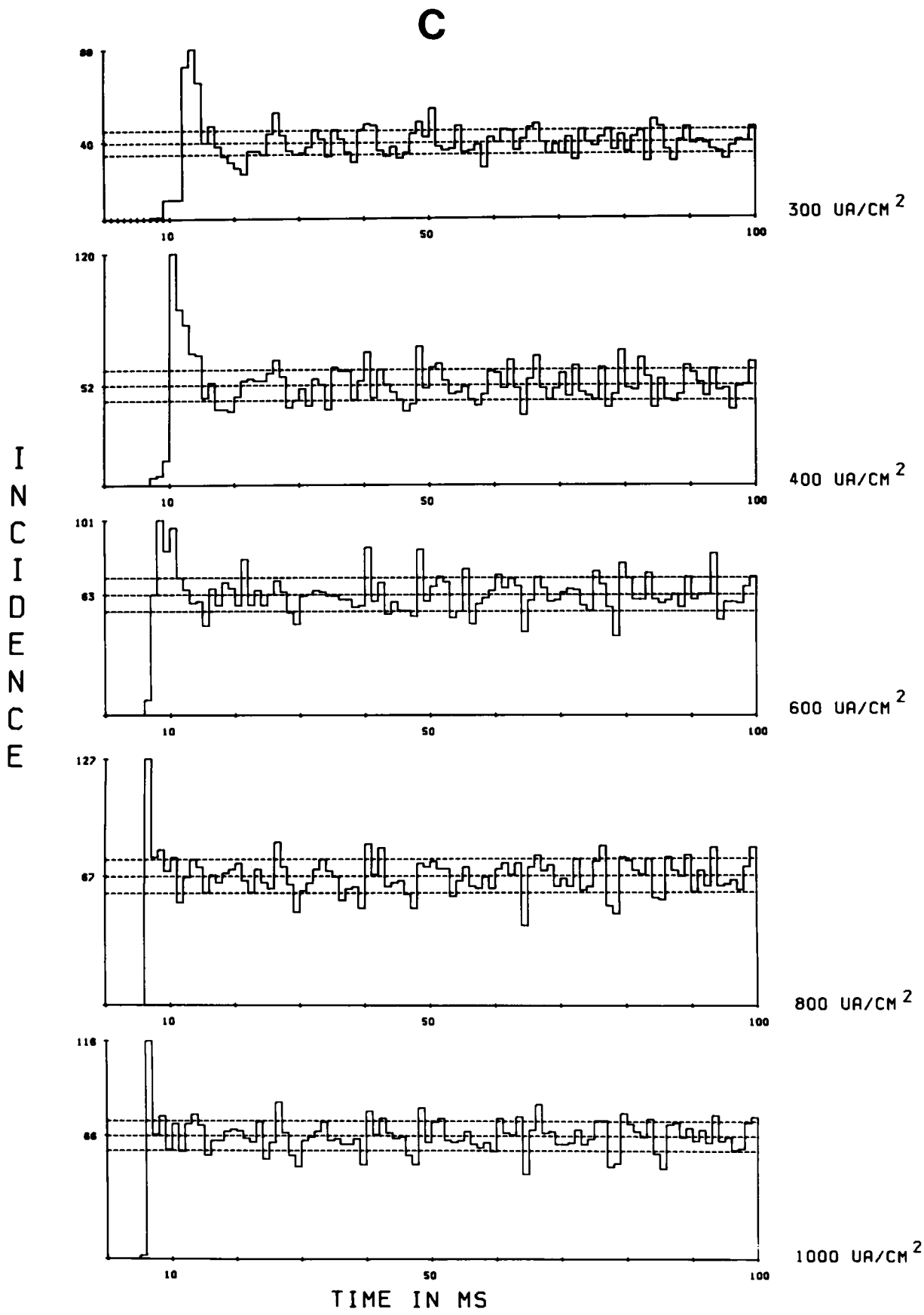
C
INCIDENCE
80
40
10
50
100
300 UA/CM 2
120
52
400 UA/CM 2
101
63
600 UA/CM 2
127
67
800 UA/CM 2
116
66
1000 UA/CM 2
TIME IN MS

FIG. 5 con't.

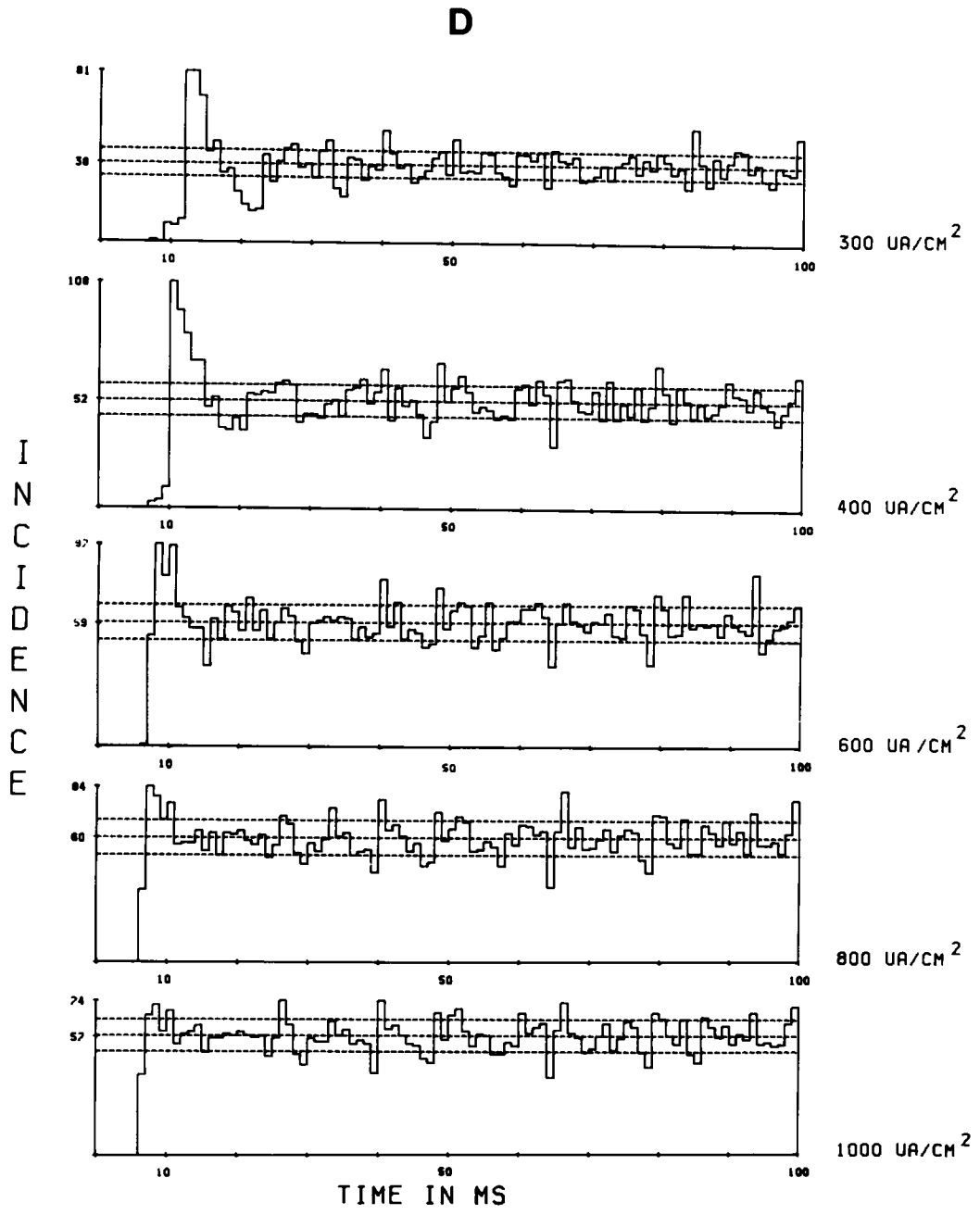

FIG. 5 con't.

$\mu A/cm^2$), curves from duration variability only and dual-parameter variability nearly converged.

Stimulus variability also effected the sequence of impulse initiation. Effects by amplitude variability are shown in Fig. 8. In each case, the pairs of responses had similar deadtimes and steady-state (i.e., T = 50–100 ms) *ED* trajectories. The differences resided in the generation of the shortest interimpulse intervals. Amplitude variability attenuated the early *ED* transient, which occurred with no amplitude variability. With amplitude variability, the prevalence of smaller amplitude stimuli limited the probability of impulse initiation following the deadtime. However, at the lowest stimulus amplitude tested, the low-rate impulse train contained fewer short interimpulse intervals and thus, on the average, elicited less post-impulse residual relative refractoriness. Under such conditions, the *ED* trajectory rose faster than occurred with no variability (Fig. 8, top). Generally, larger maximal stimuli shortened the time course of the *ED* trajectory to the plateau level.

By contrast, variability of stimulus duration yielded different sequences of impulse initiation, as shown in Fig. 9. Smaller maximal stimuli elicited an oscillatory *ED;* larger maximal stimuli shortened the deadtime, eliminated the *ED* oscillation, and shortened the risetime of the *ED*

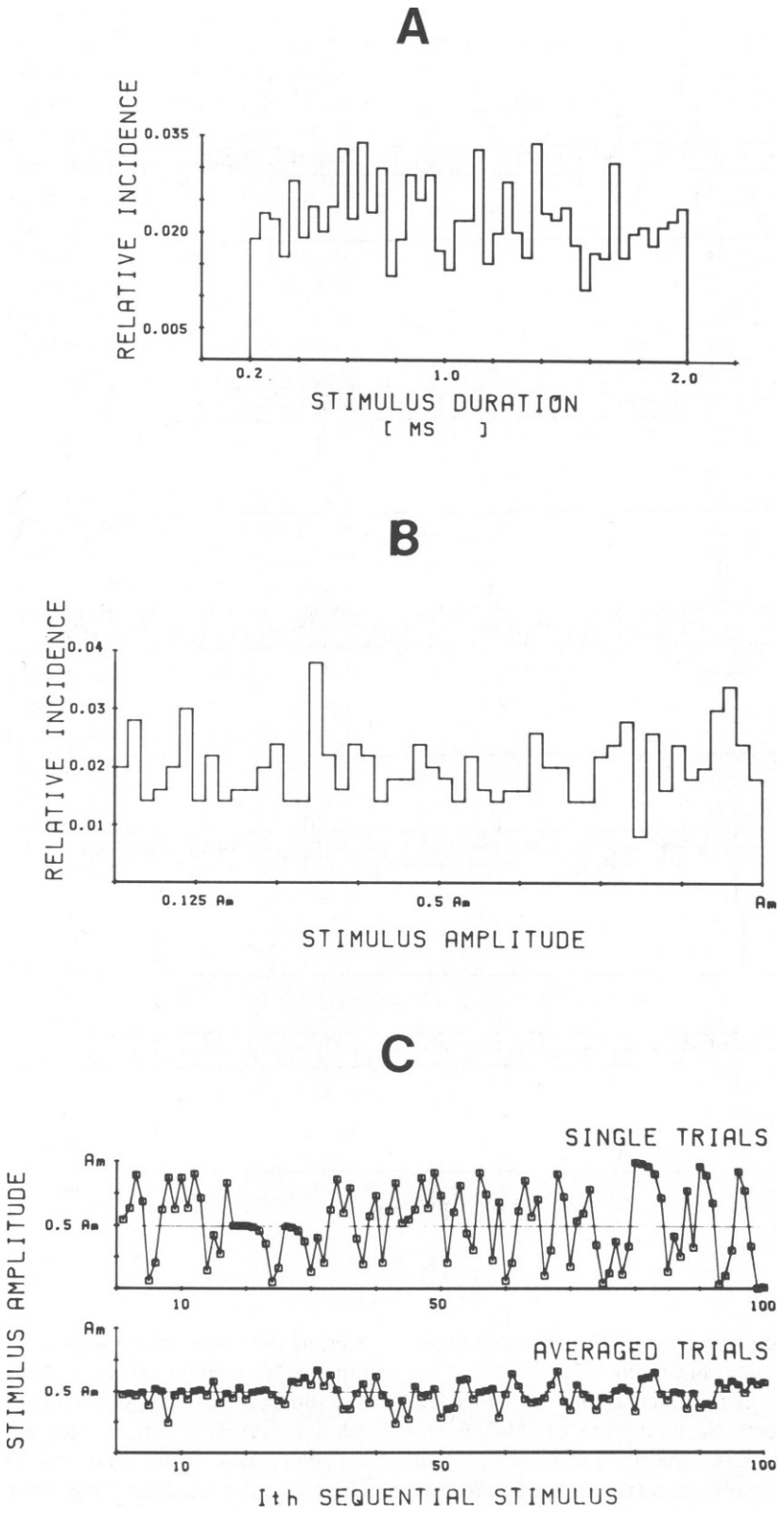

FIGURE 6 Sample distributions used to generate variability of successive stimulus pulse duration (*A*) and amplitude (*B*). (*A*) Stimulus duration distribution mean = 1.06 ms; 40 μs bins; see text for boundary explanation. (*B*) Stimulus amplitude distribution mean = 0.5 · Am; binwidth = 0.02 · Am, where Am is maximal amplitude value of a given run. (*C*) Sample of sequential variability, illustrated for amplitude parameter. Value of the Ith stimulus pulse amplitude (ordinate) plotted as 100 successive single trials (*C, top*) or as averaged value during 10 successive 100-single-trial episodes (*C, bottom*).

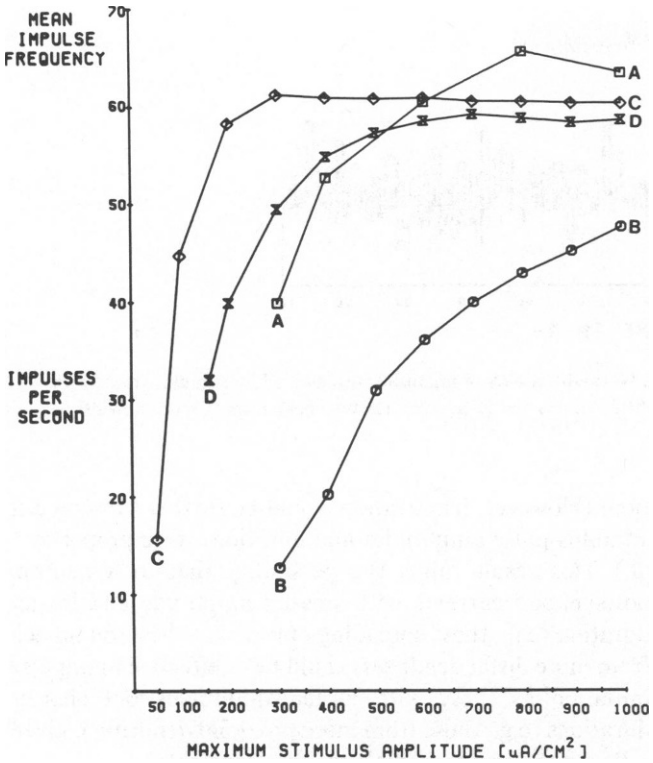

FIGURE 7 Effects of maximal stimulus amplitude on mean impulse frequency. (*A*) no variability (replotted from Fig. 3 *B*). (*B*) amplitude variability only. (*C*) Duration variability only. (*D*) Both amplitude and duration variability. For this and all subsequent figures, $Z = 2$.

trajectory to the plateau level. This was the same effect observed in *ED*s with no stimulus variability (see Fig. 5 *C*), despite the disparity in mean impulse frequency introduced by such duration variability (Fig. 7).

The effects of dual-parameter variability on impulse initiation sequence are illustrated in Fig. 10. The comparison was with runs obtained with amplitude-only variability. Thus, the addition of duration variability enhanced the generation of intervals just longer than absolute refractoriness and shortened the rise time of the *ED* trajectory to the plateau level. Neither dual-parameter variability nor amplitude-only variability supported early *ED* oscillations at the lowest maximal stimulus amplitudes.

DISCUSSION

The computed data presented were highly specific. Only one stochastic input process (Poisson) has been studied, and that at only one mean rate (98/s). The modeling of neuronal convergence as yielding a discrete-time Poisson process of identical stimulus events represented the simplest initial approach. Amplitude and temporal summations of finite-duration convergent events (Calvin, 1975) represent the next level of model complexity.

As a first approximation of responses elicited by amplitude and temporal stimulus variations, computations were performed with variability of stimulus amplitude, duration, or both. Duration variability alone greatly potentiated

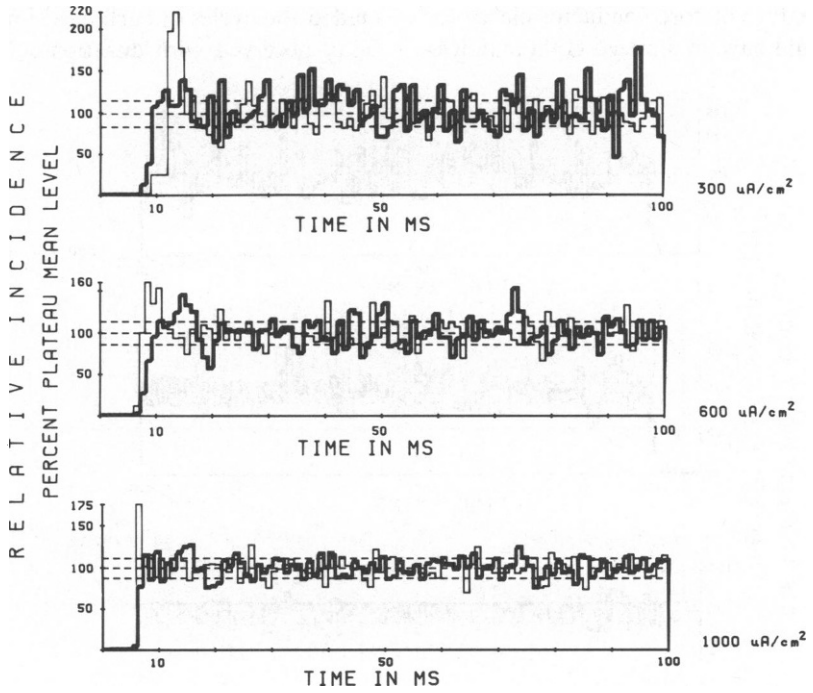

FIGURE 8 Effects of stimulus amplitude variability on impulse initiation sequence. In this and subsequent Figures, *ED* ordinates were normalized to the mean steady-state (plateau) value ($T = 50$–100 ms), with ordinate mean and $+/-1$ SD. levels shown as dashed horizontal lines. Maximal stimulus amplitudes indicated at right. Each plot shows normalized *ED* of impulse train elicited by no variability (thin lines) and by amplitude variability (heavy lines). Binwidth = 1 ms.

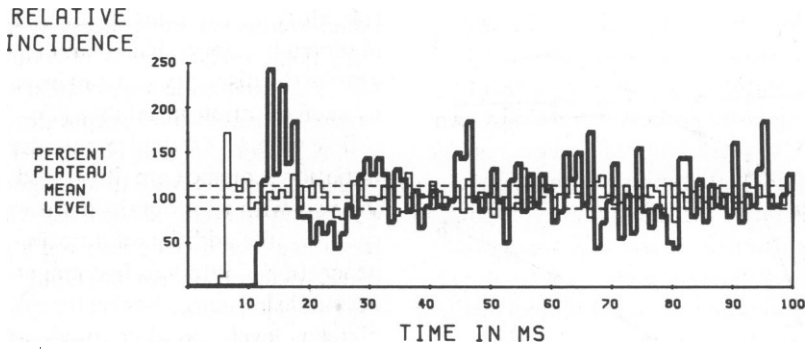

FIGURE 9 Effects of stimulus duration on impulse initiation sequences. Normalized *ED*s of impulse trains elicited by stimulus trains with duration variability only. Maximal stimulus amplitudes were 500 $\mu A/cm^2$ (thin lines) and 25 $\mu A/cm^2$ (heavy lines), respectively. Binwidth = 1 ms.

short interimpulse interval generation. With relatively short stimulus durations, this effect was expected, as stimulus duration promoted charge accumulation by the distributed cable capacitance, and yielded greater residual depolarization with longer stimulus pulse durations. Apparently, under Hodgkin-Huxley kinetics and Poisson stimulation at 98/s, the residual GNa activation on the average exceeded residual inactivation. However, with longer stimulus durations (ie, >2 ms), the opposite effect may occur as residual inactivation becomes dominant.

In the present computations, the combination of duration and amplitude variability yielded impulse frequencies greater than those that occurred with amplitude-only variability. The inverse relation between amplitude and duration (an intrinsic feature of core-conductor electrotonus) on the average should have minimized GNa inactivation. (However, inactivation would be further promoted if stimulus pulse amplitudes and durations were proportional.) This result raises the possibility that in a neuron, postsynaptic currents with smaller amplitude and longer duration (e.g., those spreading outward at the axon hillock from more distal dendrites) could be as effective in impulse initiation as those with larger amplitudes but shorter durations (e.g., those from more proximal dendrites), given a Poisson sequence of such current transients.

Effects of stimulus variability on impulse initiation sequence were assessed independently from mean impulse rate using the normalized *ED* functions (Figs. 8–10). Duration variability elicited patterns similar to those observed with no variability. Amplitude variability precluded the cycles of early post-impulse conditional probability observed with duration-only variability or with no

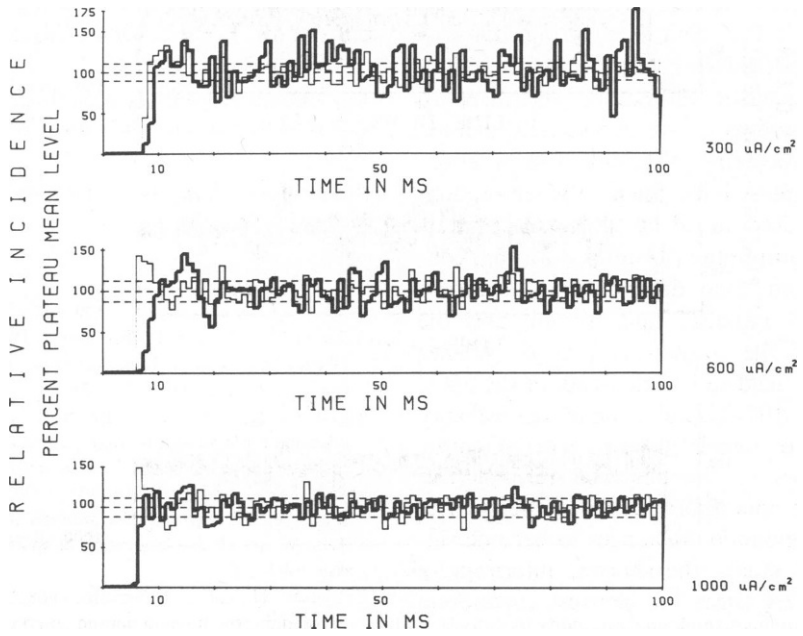

FIGURE 10 Effects of dual-parameter variability on impulse initiation sequences. Normalized *ED*s of impulse trains elicited by amplitude variability only (heavy lines) and by amplitude-and-duration variability (thin lines). Maximal stimulus amplitudes indicated at right. Binwidth = 1 ms.

variability. The combination of amplitude-and-duration variability elicited intermediary *ED* trajectories, which showed rapid rises to the plateau level but very little of the short-interval conditioning effects observed with duration-only variability or with no variability. However, in the steady-state (i.e., $T > 50$ ms), all impulse trains elicited—with or without stimulus pulse shape variability—showed the same Poisson-like pattern of a noisy but essentially constant-envelope sustained plateau level.

The model of excitable membrane cable requires further modifications to represent additional parameters of significance in impulse initiation threshold and recovery. These include the activity-dependent accumulation of extracellular K^+ (Adelman and FitzHugh, 1975), faster or slower K^+ (Connor and Stevens, 1971; Krylov and Makovsky, 1978) and other (Crill and Schwindt, 1983) ionic conductance regimes, cable morphological variations (Hillman, 1979; Horwitz, 1983; Moore et al., 1983); anodal excitation (Hodgkin and Huxley, 1952; Goldfinger, 1971; Fitz-Hugh, 1976; Faber and Horn, 1983; Jahnsen and Llinas, 1984), the role of membrane noise (Verveen and Derksen, 1965; Calvin and Stevens, 1968; Lecar and Nossal, 1971; Bryant and Segundo, 1976; French, 1984*a*; Tuckwell et al., 1984), and the cable configuration (Goldman and Albus, 1968; Funch and Faber, 1984; Blight, 1985) and conductance channel distributions (Waxman and Ritchie, 1985) of myelinated axons. Also, the kinetics and associated epiphenomena (activation, inactivation) of the macroscopic currents described empirically by Hodgkin and Huxley (1952) need to be expressed in terms of the opening/closing characteristics of their constituent single-channel currents (cf. Horn and Vandenberg, 1984).

All of the seemingly probabilistic responses were in fact entirely unprobabilistic. The computed firing patterns reflected dynamic properties underlying the ionic conductance regimes. The stochastic estimators were used to provide averaged descriptions of mathematically defined cycles of refractoriness recurring at the site of stimulation. The effectiveness for impulse initiation by a given random stimulus sequence was determined by the complex interplay between stimulus amplitude, stimulus duration, conditioning of voltage and time dependent conductance parameters by previous impulses and stimuli, and the stochastic properties of the stimulus sequence. Neither impulse reflection from the distal 'sealed-end' of the cable (Goldstein and Rall, 1974) nor conduction velocity changes as a function of interimpulse interval (George, 1977) were contributors to the observed results. The former occurs only with nonuniform cable geometry. The latter requires larger conduction distances to become significant; in the present study, the shortest interimpulse interval (4.8 ms) was 2.4 times the shortest conduction time (1.99 ms) in the longest cable considered ($Z = 3$).

While the convergence of periodic and aperiodic sequences of discrete time events readily yields a Poisson process, absolute and relative refractoriness precluded a recapitulation of this process at the output. Under certain conditions, refractoriness introduced transient periodicity (i.e., *ED* early trajectory oscillations) within the otherwise random (Poisson-like) output process. This transformation was a property of the Hodgkin-Huxley formalism, but it was also a property of an analogous but simpler formalism consisting merely of a fixed threshold criterion, brief absolute refractory period, and a subsequent longer period of relative refractoriness (Goldfinger and Fukami, 1981; Goldfinger, 1984*a*).

These computations suggest two concepts for the assessment of the axonal contribution to Poisson or quasi-Poisson neuronal firing patterns (e.g., Goldfinger and Amassian, 1980). First, the mean rate may not reflect the stimulus amplitude of the process that drives the axon, since some larger stimulus amplitudes yielded a smaller mean firing rate (Fig. 3 *B, C*). Second, ordering in the firing pattern (i.e., the *ED* trajectory) can be modified by stimulus amplitude (with or without stimulus variability within the Poisson train); the delay to the early *ED* transient was decreased by increasingly larger stimulus amplitudes. Poisson (or Poisson-like) stimulus trains have been used for experimental purposes (e.g., Redman and Lampard, 1968; Krausz, 1975; Sclabassi et al., 1982; Goldfinger et al., 1983; Craig and Tapper, 1985). Neuronal substrates in which analogue sources (i.e., PSPs, generator potentials) drive an output axon can be thus tested, where Poisson stimulation sequences activate the analogue sources and the output axonal impulse trains are recorded. If increasing stimulus amplitude does not change the *ED* pattern timing as described, such a result would be consistent with the hypothesis that an axon with Hodgkin-Huxley-like kinetics is not determining the ordering in the impulse initiation pattern (cf. French, 1984*b*; Goldfinger, 1984*b*).

This work was supported by grants from the School of Medicine and the College of Science and Engineering, Wright State University, Dayton, OH.

Received for publication 22 October 1985 and in final form 23 January 1986.

REFERENCES

Adelman, W. J., and R. FitzHugh. 1975. Solutions of the Hodgkin-Huxley equations modified for potassium accumulation in a periaxonal space. *Fed. Proc.* 34:1322–1329.

Blight, A. R. 1985. Computer simulations of action potentials and afterpotentials in mammalian myelinated axons: The case for a lower resistance myelin sheath. *Neuroscience.* 15:13–31.

Bryant, H. L., and J. P. Segundo. 1976. Spike initiation by transmembrane current: a white noise analysis. *J. Physiol. (Lond.)* 260:279–315.

Calvin, W. H. 1975. Generation of spike trains in CNS neurons. *Brain. Res.* 84:1–22.

Calvin, W. H., and C. F. Stevens. 1968. Synaptic noise and other sources of randomness in motoneuron interspike intervals. *J. Neurophysiol.* 31:574–587.

Connor, J. A., and C. F. Stevens. 1971. Prediction of repetitive firing behaviour from voltage clamp data on an isolated neurone soma. *J. Physiol. (Lond.)* 213:31–53.

Cox, D. R., and P. A. W. Lewis, 1966. The Statistical Analysis of Series of Events. (Methuen (London). 285 pp.

Cox, D. R., and H. D. Miller. 1965. The Theory of Stochastic Processes. Methuen (London). 398 pp.

Cox, D. R., and W. L. Smith. 1953. The superposition of several strictly periodic sequences of events. *Biometrika.* 40:1–11.

Craig, A. D., and D. N. Tapper. 1985. A dorsal spinal neural network in cat. III. Dynamic nonlinear analysis of responses to random stimulation of single Type 1 cutaneous input fibers. *J. Neurophysiol.* 53:995–1015.

Crill, W. E. and P. C. Schwindt. 1983. Active currents in mammalian central neurons. *Trends Neurosci.* 60:236–240.

Faber, D. S., and H. Korn. 1983. Field effects trigger post-anodal rebound excitation in vertebrate CNS. *Nature (Lond.).* 305:802–804.

FitzHugh, R. 1976. Anodal excitation in the Hodgkin-Huxley nerve model. *Biophys. J.* 16:209–226.

French, A. S. 1984*a*. The frequency response function and sinusoidal threshold properties of the Hodgkin-Huxley model of action potential encoding. *Biol. Cybern.* 49:169–174.

French, A. S. 1984*b*. Dynamic properties of the action potential encoder in an insect mechanosensory neuron. *Biophys. J.* 46:285–290.

Funch, P. G., and D. S. Faber. 1984. Measurement of myelin sheath resistances: implications for axonal conduction and pathophysiology. *Science (Wash. DC).* 225:538–540.

George, S. A. 1977. Changes in interspike interval during propagation: quantitative description. *Biol. Cybern.* 26:209–213.

Goldfinger, M. D. 1971. Anode-break excitation: a formalistic calculation. *Biol. Bull.* 141:387.

Goldfinger, M. D. 1978. Propagated responses in nerve and muscle cable models. *Brain Theory Newsletter.* 3:63–65.

Goldfinger, M. D. 1984*a*. Superposition of impulse activity in a rapidly-adapting afferent unit model. *Biol. Cybern.* 50:385–394.

Goldfinger, M. D. 1984*b*. Responses of cat G1 hair receptors to random-sequence stimulus trains. *Soc. Neurosci. Abstr.* 10:109.

Goldfinger, M. D., and V. E. Amassian. 1980. Response of forelimb guard hair afferent units to airjet stimulation of the entire receptive field. *J. Neurophysiol.* 44:961–978.

Goldfinger, M. D., and Y. Fukami. 1981. Interaction of activity in frog skin touch afferent units. *J. Neurophysiol.* 45:1096–1108.

Goldfinger, M. D., Kuo, W., and K. P. Zimmermann. 1983. Poisson-electrical stimulation of an axonal bundle. *Soc. Neurosci. Abstr.* 9:1194.

Goldman, L., and J. S. Albus. 1968. Computation of impulse conduction in myelinated fibers: theoretical basis of the velocity diameter relation. *Biophys. J.* 8:596–607.

Goldstein, S. S. and W. Rall. 1974. Changes in action potential shape and velocity for changing core conductor geometry. *Biophys. J.* 14:731–757.

Griffith, J. S. 1971. Mathematical Neurobiology. Academic Press, Inc., NY. 49–53.

Hillman, D. E. 1979. Neuronal shape parameters and substructures as a basis of neuronal form. The Neurosciences Fourth Study Program. F. O. Worden and F. O. Schmitt, editors. MIT Press, Cambridge, MA. 477–497.

Hines, M. 1984. Efficient computation of branched nerve equations. *Int. J. Bio-Med. Comput.* 15:69–76.

Hodgkin, A. L., and A. F. Huxley. 1952. A quantitative description of membrane current and its application to conduction and excitation in nerve. *J. Physiol. (Lond.).* 117:500–544.

Horn, R., and C. A. Vandenberg. 1984. Statistical properties of single sodium channels. *J. Gen. Physiol.* 84:505–534.

Horwitz, B. 1983. Unequal diameters and their effects on time varying voltages in branched neurons. *Biophys. J.* 41:51–66.

Jahnsen, H., and R. Llinas. 1984. Ionic basis for the electroresponsiveness and oscillatory properties of guinea-pig thalamic neurons in vitro. *J. Physiol. (Lond.).* 349:227–247.

Krausz, H. I. 1975. Identification of nonlinear systems using random impulse train inputs. *Biol. Cybern.* 19:217–230.

Krylov, V. B., and V. S. Makovsky. 1978. Spike frequency adaptation in amphibian sensory fibres is probably due to slow K channels. *Nature (Lond.).* 275:549–551.

Lecar, H., and R. Nossal. 1971. Theory of threshold fluctuation in nerves. I. Relationships between electrical noise and fluctuations in axonal firing. *Biophys. J.* 11:1048–1067.

Moore, J. W., N. Stockbridge, and M. Westerfield. 1983. On the site of impulse initiation in a neurone. *J. Physiol. (Lond.).* 336:301–311.

Poggio, G. F., and L. J. Viernstein. 1964. Time series analysis of impulse sequences of thalamic somatosensory neurons. *J. Neurophysiol.* 27:517–545.

Pumphrey, R. J., and J. Z. Young. 1938. The rates of conduction of nerve fibres of various diameters in cephalopods. *J. Exp. Biol.* 15:453–467.

Rall, W. 1977. Core conductor theory and cable properties of neurons. *in* Cellular Biology of Neurons. Vol. I. Handbook of Physiology—The Nervous System. I. J. M. Brookhart and V. B. Mountcastle, editors. Amer. Physiol. Soc. Bethesda, MD. 39–97.

Redman, S. J., and D. G. Lampard. 1968. Monosynaptic stochastic stimulation of cat spinal motoneurons. I. Response of motoneurons to sustained stimulation. *J. Neurophysiol.* 31:485–498.

Roberts, A., and B. M. H. Bush, editors. 1981. Neurons without impulses. *Soc. Exp. Biol. Sem. Ser.* No. 6. 290 pp.

Sclabassi, R. J., J. K. Vries, and D. M. Bursick. 1982. Somatosensory evoked potentials to random stimulus trains. *Ann. NY. Acad. Sci.* 388:695–701.

Tuckwell, H. C., F. Y. M. Wan, and Y. S. Wong. 1984. The interspike interval of a cable model neuron with white noise input. *Biol. Cybern.* 49:155–167.

Verveen, A. A., and H. E. Derksen. 1965. Fluctuations in membrane potential and the problem of coding. *Kybernetik.* 2:152–160.

Waxman, S. G., and J. M. Ritchie. 1985. Organization of ionic channels in the myelinated nerve fiber. *Science (Wash. DC).* 228:1502–1507.